Automated Analysis of Holointerferograms for the Determination of Surface Displacement

by D.R. Matthys, T.D. Dudderar and J.A. Gilbert

ABSTRACT—A method for using an image digitizing system with a minicomputer to automatically determine surface-displacement fields by evaluating holographic fringe patterns is presented. The problem of determining the sign of the displacement vector as well as the need to produce a monotonic phase change across the surface under observation is solved by utilizing the method of carrier fringes. A set of programs has been written so that the camera/computer system can view the pattern of deformation-modulated carrier fringes and, with a knowledge of the initial carrier-fringe pattern, draw a profile plot of the deformed surface. The procedure is exemplified with a study of a centrally loaded disk.

Introduction

Although interferometry is sometimes said to be one of the most significant applications of holography,[1] it is in fact rarely found in actual industrial settings. There are several reasons for this, including the need for vibration isolation of the system, the complexity of the required optical setup, and the problems of using a photographic darkroom process. But probably the major factor inhibiting full exploitation of holographic interferometry as a precision noncontact full-field measurement tool is the difficulty of getting quantitative results out of the interferograms.

Current developments in holographic techniques have made it possible to alleviate many of these difficulties, e.g., high-power pulsed lasers can remove the need for vibration isolation, fiber-optic cables and bundles can greatly simplify optical setups and allow holographic measurements in remote or inaccessible locations,[2] and special holographic cameras are now available that do not require darkroom procedures and which produce holographic images *in situ* within a few seconds.

In spite of these technical advances, quantitative holographic interferometry has not found widespread application. The real root of the problem lies in the fact that the interference patterns obtained in practical cases are frequently so complex that a skilled analyst cannot easily derive quantitative results from them. Moreover, the interferogram does not contain sufficient information to determine the sign of a surface displacement, i.e., whether the surface has moved towards or away from the observer. Heretofore, most efforts to use digital methods in the study of holointerferograms have been limited to the analysis of basically linear fringe distributions due to simple translations or nearly uniform deformations;[3-7] but little effort has been directed toward solving these fundamental problems. However, if holography is to become a commonly used measurement tool, some method of simplifying the analysis of reasonably complex interferograms must be developed. The goal of the work described in this paper is to show that by combining image digitization with computerized analysis, this simplification can in fact be attained through the use of carrier fringes. The introduction of carrier fringes into holographic-interference-fringe patterns is not new;[8-10] but the present work describes the successful application of sophisticated image digitization techniques, carrier fringes, fiber optics, and computer coding into a unified system for automatic fringe analysis.

The main advantages of the carrier-fringe technique are that it removes the sign ambiguity ordinarily present in interferometric fringe patterns and that it also imposes monotonicity on the phase change across an object surface so that an automated system may be used for analysis. Computer codes have been developed to analyze the fringe patterns so that it is now feasible to design a system which, given knowledge of the carrier-fringe pattern, can automatically evaluate the holointerferometric fringes on the deformed surface and produce a plot of displacements of that surface.

To develop and test such an automated system, it was decided to map the surface deflection of a centrally loaded linear-elastic disk. This is a familiar test specimen. The results are known from theory; and the interference patterns obtained from such a test object are neither trivial nor excessively complex. A photograph of the interference pattern obtained by making a double-exposure hologram of a disk before and after applying central loading is shown in Fig. 1. The interference fringes are basically just a set of concentric rings. Note that it is impossible to determine the direction of surface deflection from study of the holointerferogram alone. The

D.R. Matthys (SEM Member) is Associate Professor, Marquette University, Physics Department, Milwaukee, WI 53233. T.D. Dudderar (SEM Fellow) is Member of Technical Staff, AT&T Bell Laboratories, Room 1A-105, 600 Mountain Avenue, Murray Hill, NJ 07974. J.A. Gilbert (SEM Member) is Professor, University of Alabama in Huntsville, Department of Mechanical Engineering, Huntsville, AL 35899.

Paper was presented at the 1985 SEM Spring Conference on Experimental Mechanics held in Las Vegas, NV on June 9-14.

Original manuscript submitted: August 26, 1986. Final manuscript received: June 29, 1987.

disk may be bowed either inward or outward. Also, the curved fringes are difficult to interpret by automated analysis because of the problem of programming the computer to enable it to detect when the same fringe is being encountered in a different location. Unfortunately, without some method for uniquely identifying each fringe, the computer may count each of them more than once during a scan across the disk face. One method to obviate this problem (without invoking operator interaction) is to incorporate an initial carrier-fringe pattern with a higher spatial frequency than any expected from the deformation-modulated carrier-fringe pattern. Figure 2 shows the appearance of the unloaded disk when carrier fringes are created in the holographic image. In this case the fringes were generated by tilting the disk, but in fact the carrier pattern could have been generated by changing the orientation of the illumination, the reference beam, or the hologram itself.[11]

The governing equation for holographic displacement analysis on a diffuse surface is

$$(\hat{e}_1 - \hat{e}_2) \cdot d = n\lambda \tag{1}$$

where d is the displacement vector, n is the fringe order, and λ is the wavelength. For each point on the test surface, $\hat{e}_1$ and $\hat{e}_2$ are unit vectors drawn from the source to the point and from the point to the observation position, respectively.

The quantity $(\hat{e}_1 - \hat{e}_2) \cdot d$ is often referred to as the projected displacement d_p.

The carrier pattern required for digitization can be expressed as

$$\delta = n_1\lambda \tag{2}$$

where δ is the linear phase change across the field of view and n_1 is the carrier-fringe order. To be effective these carrier fringes should be localized close to the test surface, and oriented perpendicular to the direction of scan denoted by s.

When deformation is superimposed on the carrier, the modulated fringe pattern is given by

$$(\hat{e}_1 - \hat{e}_2) \cdot d + \delta = n_2\lambda \tag{3}$$

The fringes in the holointerferograms corresponding to eqs (2) and (3) can be digitized and subtracted, and

$$(\hat{e}_1 - \hat{e}_2) \cdot d = (n_2 - n_1)\lambda = \Delta n\lambda \tag{4}$$

Equation (4) is the same as eq (1) when $n = n_2 - n_1$. The carrier pattern will facilitate digitization of the deformation-modulated carrier-fringe pattern when the fringe gradient of the carrier, $d(n_1)/ds$, meets certain conditions. Differentiating eq (4),

$$d(d_p)/ds = [d(n_2 - n_1)/ds]\lambda =$$

$$[d(n_2)/ds - d(n_1)/ds]\lambda \tag{5}$$

In eq (5), $d(d_p)/ds$ represents the rate of change of the projected displacement, and $d(n_1)/ds$ and $d(n_2)/ds$ are the slopes of the carrier and deformation-modulated fringe patterns, respectively, in plots of fringe order versus row/column number. In general, the slope of the carrier-fringe pattern, $d(n_1)/ds$, is known, and $d(n_2)/ds$ can be measured for each point along s. This uniquely specifies $d(d_p)/ds$, and hence the sign of the projected displacement is determined. When $d(n_1)/ds > 0$, the method works provided that $d(n_2)/ds$ never becomes negative. This condition must be satisfied to insure that each fringe in the modulated pattern is scanned only once, and the modulated pattern has monotonically increasing fringe orders over the scan. This condition depends on the fringe gradient in the carrier pattern; the higher the carrier-fringe density, the less likely that

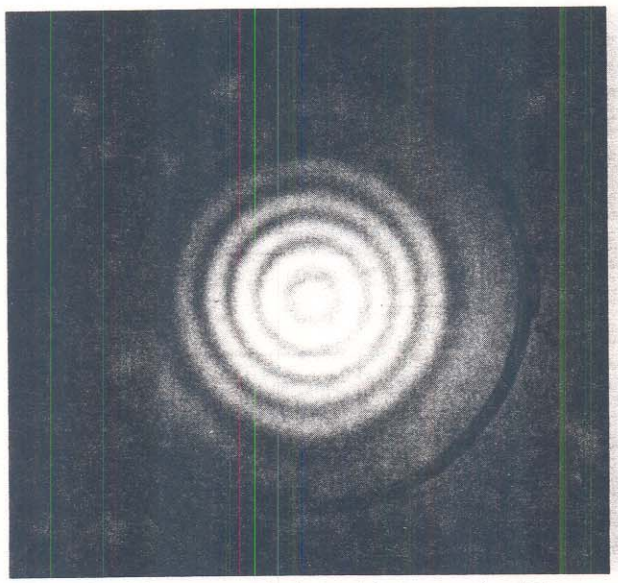

Fig. 1—Double-exposure holographic image of a disk before and after central loading showing interference fringes due to surface deformation

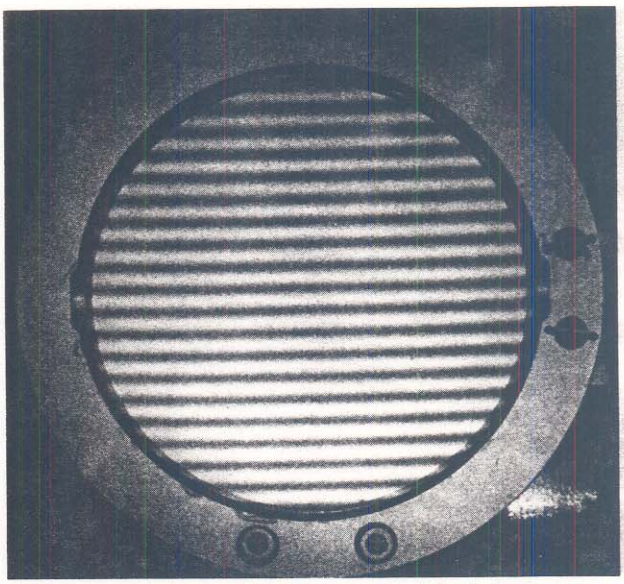

Fig. 2—Carrier-fringe pattern generated by introducing a small tilt about a horizontal diametral line across the surface of the undeformed disk. The rotation was 0.0039 deg with the bottom of the disk moving towards the observer

$d(n_2)/ds < 0$. However, the resolution of the imaging system imposes some constraints. Not only must the carrier-fringe density remain within the resolution limit, but so must that of the deformation-modulated fringe pattern.

Assigning arbitrary fringe-order numbers along a scan line uniquely establishes the sign of the projected displacement. In this case, however, the magnitude of d_p is determined to only within a constant. Absolute displacement measurement requires that absolute fringe orders be established in both the carrier and the modulated patterns. This is most easily done by initiating a known carrier thereby assigning n_1, and then following one fringe in real time as deformation occurs to determine n_2. An alternative method is to have prior knowledge of the displacement of at least one point in the deformation-modulated fringe field. For example, a point lying on a fixed boundary will have the same fringe order in the carrier and deformation-modulated carrier-fringe patterns.

In this experiment, the disk was tilted about a horizontal axis through the center of the disk surface, with the bottom of the disk being moved toward the observer. Since the direction of the tilt is known, the sign of the fringe orders can be assigned unambiguously; the carrier-fringe-order numbers are increasing toward the bottom of the disk and decreasing toward the top. The zero order fringe is located directly above the rotation axis.

Figure 3 shows the appearance of the fringe pattern when a holointerferogram of the disk is recorded with both carrier and deformation present. Note that no fringe appears twice when counted along a vertical line from bottom to top anywhere along the disk. The effect of the deformation fringes is to merely expand or compress the carrier-fringe spacing, so it is simple to determine whether the fringe order is increasing or decreasing. Since suitable programs are available, it is possible for the computer, equipped with a digitizing camera, to view the fringe pattern of the loaded surface and automatically draw a plot of the surface deformation of the disk.

Experimental Setup

A glass disk of 88-mm diameter and 1.6-mm thickness was bonded around its circumference to a stiff ring suspended vertically in a gimballed holder which permitted the disk to be rotated around either a vertical or horizontal axis through a surface diameter. In addition, a large micrometer was positioned behind the disk to allow the application of controlled central displacements.

Figure 4 shows the optical setup used to generate the holograms. For a symmetric arrangement with equal illumination and viewing angles (measured with respect to the surface normal), the normal displacement W is given by eq (1) which simplifies to $2W \cos \beta = n\lambda$, where β is the illumination angle, n is the fringe order, and λ is the wavelength of light used. In this test arrangement, the angle β was 4.58 degrees and the light source was a helium-neon laser, so normal or out-of-plane displacements could be measured with a fringe sensitivity of 0.317 microns. A single-mode optical fiber was used for illumination to simplify the setup.

Figure 5 is a block diagram showing the major components of the system used for this test of automated fringe reduction and surface contouring. The vidicon camera used is capable of digitizing an image with an eight-bit gray scale (256 levels) and a resolution of 1024 by

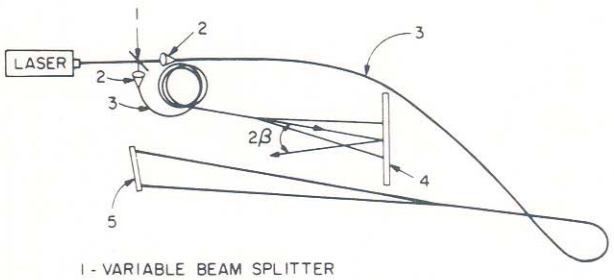

1 - VARIABLE BEAM SPLITTER
2 - FIBER LAUNCH OPTICS
3 - SINGLE MODE OPTICAL FIBER
4 - MODEL
5 - HOLOGRAM PLATE

Fig. 4—Optical setup for taking holograms of the disk. The arrangement of the angle 2 between the illumination and viewing directions established the sensitivity vector as normal to the disk surface and allowed measurement of out of plane deformation. In this setup the value of β was 4.58 deg

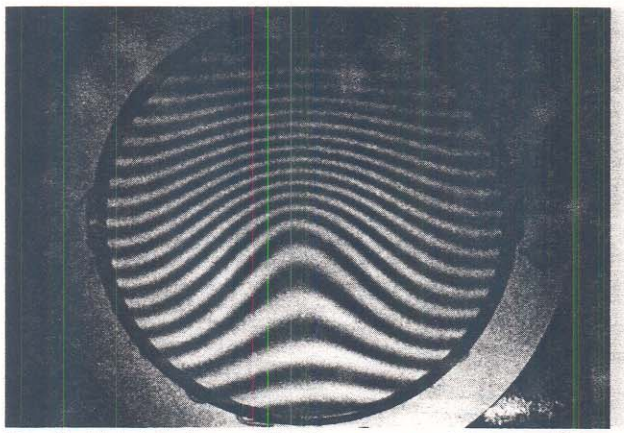

Fig. 3—Holointerferometric fringes caused by combining the carrier tilt and the deformation due to central loading of the disk. The amount of loading was 1.60 microns toward the observer

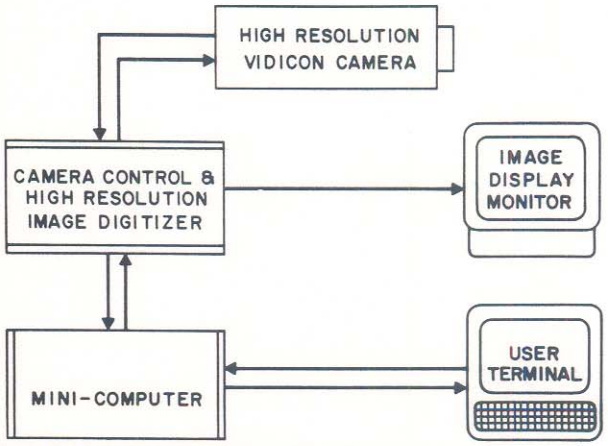

Fig. 5—Schematic showing the equipment used in the experiment

1024 pixels. A camera control allows selection of every second or every fourth row and column element, thus allowing the resolution to be reduced to 512 by 512, or 256 by 256 pixels. To reduce the size of the data files a resolution of 256 by 256 was chosen for this experiment. Consequently, the data files obtained from digitizing the holographic images were only 64K bytes in size. Such files can easily be handled by a relatively small computer, enabling the calculations involved in this experiment to be performed on a relatively inexpensive system.

Experimental Procedure

The actual data needed for this approach include only digitized holointerferometric images of (1) the unloaded disk with a carrier-fringe pattern, and (2) the loaded disk showing the deformation-modulated carrier-fringe pattern, plus knowledge of the direction of tilt used to generate the carrier-fringe pattern. Therefore the first step was to produce a suitable holointerferometric carrier pattern across the disk surface. Using a thermoplastic holocamera, a hologram was made of the unloaded disk. Then the disk was tilted 0.0039 degrees about a horizontal diametrical line across the disk surface. The direction of tilt was such that the bottom of the disk moved toward the observer. A photograph was then taken of the real-time fringe pattern generated by interference effects between the holographic image of the disk and the tilted disk surface. The resulting fringe distribution is shown in Fig. 2. The center of the disk was then displaced 1.60 microns toward the observer and another photograph of the fringe distribution on the disk surface taken. This deformation-modulated carrier-fringe pattern is shown in Fig. 3.

Data Analysis

Since the direction of tilt is known, all of the information needed to contour the deformed surface is contained in these two photographs. To enable automated analysis, the pictures were digitized using the vidicon camera as described above. The column representing the vertical center line through the disk surface, column 128 of the data arrays, was chosen to demonstrate the method of analysis.

An intensity plot of this column, scanning from bottom to top, is shown in Figs. 6(a) and 6(b) for each of the two images. Figure 6(a) shows the initial intensity variation across the unloaded, undeformed disk with its carrier fringe pattern, while Fig. 6(b) shows similar information for the loaded, deformed disk. Figure 6(a) clearly shows the edges of the disk and the basically uniform sinusoidal intensity distribution across the disk surface. In addition

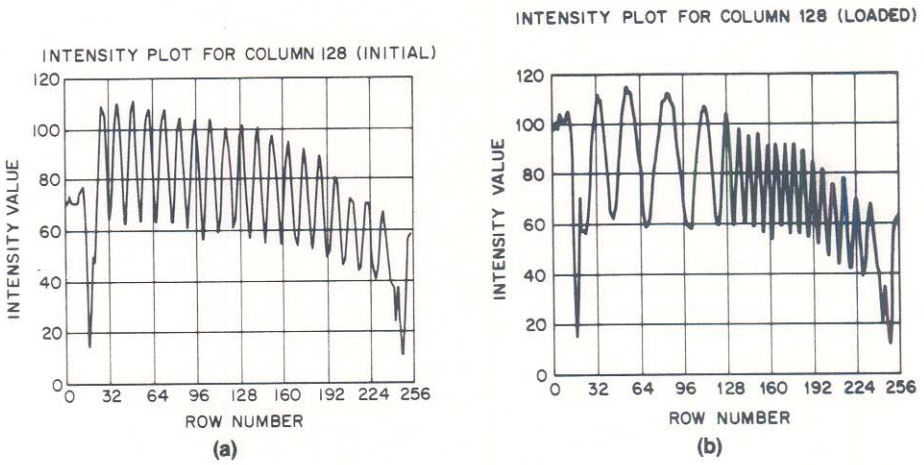

Fig. 6—(a) Intensity trace across vertical midline of the disk for fringe distribution shown in Fig. 2 (carrier fringes only). Direction of scan was from the bottom edge of the disk to the top along column 128. (b) Intensity trace across vertical midline of the disk for fringe pattern shown in Fig. 3 (carrier plus deformation). Direction of the scan was from bottom to top along column 128

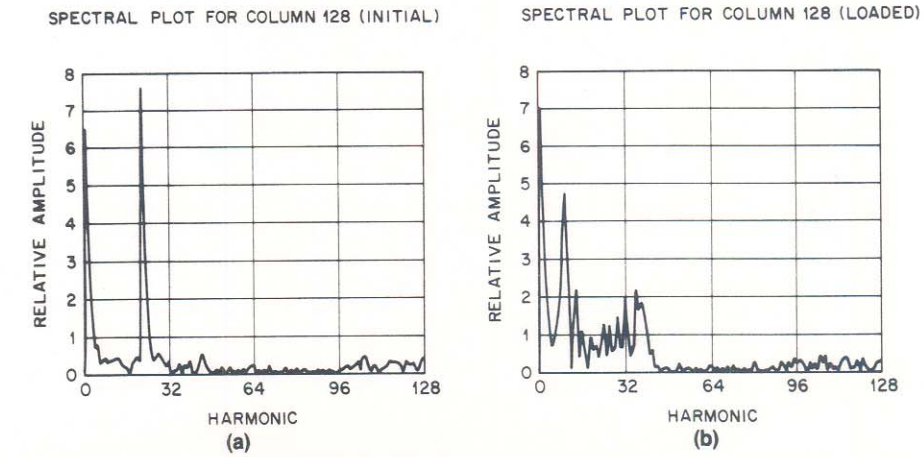

Fig. 7—(a) Spectral plot of the intensity trace given in Fig. 6(a) (carrier fringes only). The spatial harmonics were measured in terms of the 256 rows in the data array, i.e., the fundamental frequency would produce one complete cycle across the 256 rows. (b) Spectral plot of the intensity trace given in Fig. 6(b) (carrier plus deformation fringes). Spatial harmonics were measured as in Fig. 7(a)

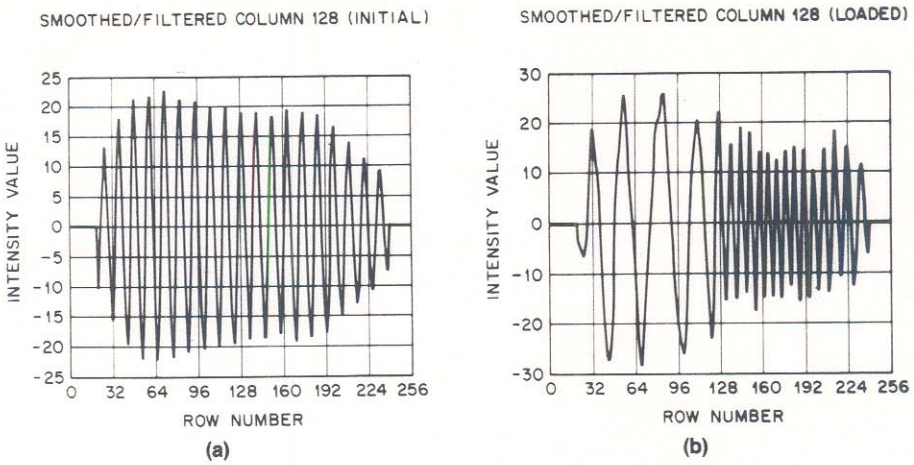

Fig. 8—(a) Filtered and smoothed version of trace given in Fig. 6(a) (carrier only). (b) Filtered and smoothed version of trace given in Fig. 6(b) (carrier plus deformation)

to the sinusoidal carrier-fringe pattern, a very low frequency intensity variation due to the Gaussian nature of the laser illumination is also evident.

The next step was to locate the edges of the disk and clip both patterns to the midpoints of the last cycle contained within these edges. Fourier transforms of the clipped patterns are shown in Figs. 7(a) and 7(b). The important characteristics of Fig. 7(a), which shows the frequency spectrum for the unloaded disk (carrier only), are the sharp peak at the carrier frequency, the very low frequency peak representing the Gaussian intensity distribution of the laser beam, and the high-frequency noise due to speckle, nonlinearities in the film, optical-system limitations, etc. Figure 7(b), which gives equivalent information for the loaded disk (carrier plus deformation), shows that the deformation information causes a frequency modulation of the original carrier pattern, with the desired information now present as a sideband of the carrier frequency. Comprehensive discussions of the use of Fourier-transform methods for the analysis of digitized holointerferometric fringe patterns have been published by Kreis.[12,13]

Working first with the spectrum of the undeformed image [Fig. 7(a)], the program set up a narrow passband centered around the carrier frequency. All frequencies outside this passband were removed. The program then examined the spectrum of the deformed image [Fig. 7(b)], and cut off the low-frequency spike which was the result of the Gaussian intensity envelope; it also removed all high frequencies where signal strength had fallen back to the noise level. The resulting spectra were then transformed back to the time domain using an inverse Fourier transform and the results are shown in Figs. 8(a) and 8(b). A low-frequency intensity variation still shows up as an envelope of the desired signals, but this is of minor importance since it is phase, not intensity, which is significant.

In order to find the fringes, the computer next proceeded to locate the extrema of the intensity distributions for each filtered fringe pattern. This was done by applying standard methods of data analysis[14] to fit curves through the data points, and then differentiating to locate the desired extrema. Since the data for each column contain a large number of points which correspond to a small number of cycles of a basically sinusoidal intensity distribution, the graph obtained by curve fitting is relatively insensitive to the specific technique used, and any standard

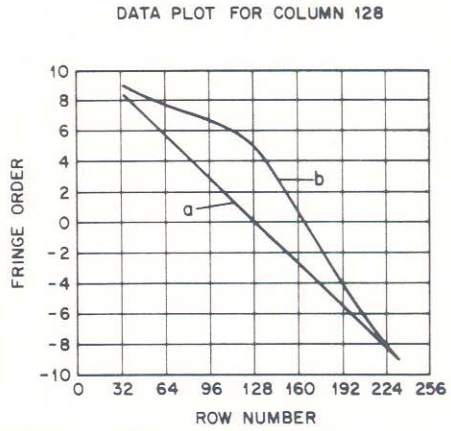

Fig. 9—Plots of the fringe order versus the row number (distance from the bottom of the disk). Curve 'a' is for the unloaded disk (carrier only), while curve 'b' is for the loaded disk (carrier plus deformation)

method should give essentially the same results. Figure 9 shows fringe-order versus row-number plots along the vertical center line (column 128) for both the unloaded and the loaded disk. The curve labeled 'a' is for the unloaded disk (carrier only) while curve 'b' is for the loaded disk (carrier plus deformation). The linear curve 'a' obtained for the unloaded case is simply a manifestation of the simple sinusoidal pattern of fringes across the face of the disk and the zero-order fringe is located at the disk center, over the rotation axis. In curve 'b', for the loaded condition, there is a slow phase change across the lower part of the disk where the intensity fringes were spaced out, and then a rapid phase change across the upper part of the disk where the fringes were crowded together.

Since curve 'a' of Fig. 9 gives information concerning the phase-change distribution due to the carrier while curve 'b' of the same figure gives the corresponding information for the deformation-modulated carrier, the next step in the process was to subtract the two curves. Since the data represent extrema occurring at different row locations in the two curves, the data will have to be interpolated first. Because the curves are smooth with respect to the spacing between data points, the choice of

interpolation method is not critical. For this experiment, a cubic-spline technique[15] was used to interpolate values for each row of the two curves, and these values were then subtracted from each other to get the distribution of phase change due to the deformation alone. In addition, a phase change of zero was imposed at the edges of the disk where the disk was bonded to its support ring. This result is shown in Fig. 10, which is a profile plot of the out-of-plane deformation of the disk surface across the vertical center line from bottom to top.

Automated repetition of the preceding analysis for each digitized column provides a full-field description of the out-of-plane deformation of the disk as desired. This final result is given in Fig. 11, which shows a perspective plot of the deformed disk obtained from the computer-graphics output.

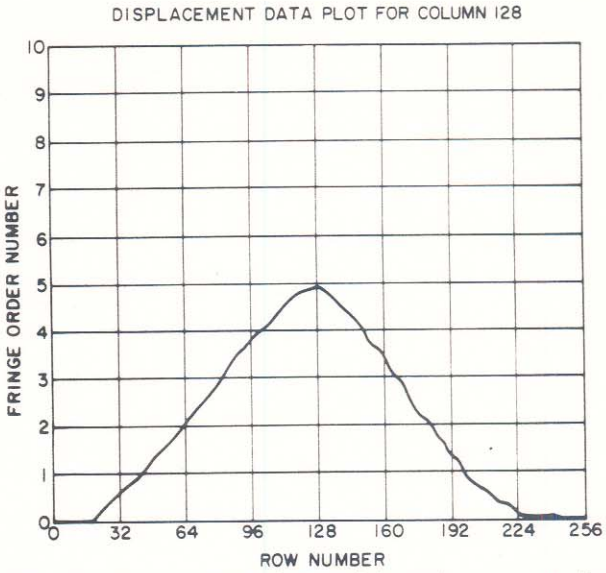

Fig. 10—Contour map of the disk surface across the vertical center line of the disk, obtained by subtracting the fringe-order distributions shown in Fig. 9(a) and 9(b)

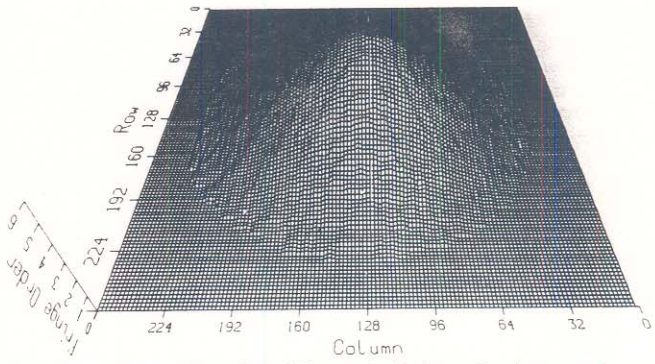

Fig. 11—Perspective plot of the out of plane displacement as derived directly from the computer-plotter output

Summary

The method of carrier fringes was successfully applied in this study of a centrally loaded disk. The carrier fringes resolved the problem of sign ambiguity and linearized the fringes so that the phase shift across the disk surface was monotonic, thus allowing automatic scanning. Computer programs incorporating Fourier-transform filtering were written to analyze the holointerferometric fringes on the surface of the loaded disk. Since the computer knew the details of the carrier pattern, it was possible for the computer to draw a profile plot of the out-of-plane deformation.

The method could be extended to dynamic studies if a high-speed camera were available. Though the time required for analysis of each image precludes real-time studies of dynamic changes, a high-speed camera could be used to record the changing fringes and selected frames could be digitized and studied later. Note that the carrier image information need be given to the computer just once, and all other images need only contain information about the deformation-modulated carrier-fringe patterns.

Acknowledgments

Major funding for this work was provided by the U.S. Army Research Office under Contract Nos. DAAG 29-84-K-0183, DAAG 29-84-G-0045 and DAAL 03-86-K-0014. The authors also wish to thank AT&T Bell Laboratories, Murray Hill, NJ for its support.

References

1. Jones, R. and Wykes, C., "Holographic and Speckle Interferometry," 64, Cambridge Press, New York (1983).

2. Dudderar, T.D. and Gilbert, J.A., "Real-Time Holographic Interferometry through Fiber Optics," J. Phys. Eng.: Sci Instr., **18**, 39-43 (1985).

3. Katzir, Y., Glaser, I., Friesem, A.A. and Sharon, B., "On-Line Acquisition and Analysis for Holographic Nondestructive Evaluation," Opt. Eng., **21**, 1016-1021 (1982).

4. Hot, J.P. and Durou, C., "System for the Automatic Analysis of Interferograms Obtained by Holographic Interferometry," SPIE 2nd European Cong. on Optics Applied to Metrology, **210**, 144-151 (1979).

5. Lamy, F., Liegeois, C. and Meyrueis, P., "Automatic Computer Analysis of Double Exposure Holograms in Industrial Nondestructive Control," Proc. SPIE, **353**, 82-89 (1983).

6. Kreis, T.M. and Kreitlow, H., "Digital Processing of Holographic Interference Patterns," OSA/SESA Topical Mtg. on Hologram Interferometry and Speckle Metrology, Cape Cod, MA, Paper No. TuB2 (June 1980).

7. Lanzl, F. and Schluter, M., "Microprocessor-Controlled Hologram Analysis," IEEE 5th Int. Computing Conf., London, 159-162 (1978).

8. Katzir, Y., Friesem, A.A., Glaser, I. and Sharon, B., "Holographic Nondestructive Evaluation with On-Line Acquisition and Processing," Industrial and Commercial Applications of Holography, ed. M. Chang, Proc. SPIE, **353**, 74-81 (1982).

9. Sciammarella, C.A. and Ahmadshahi, M., "Computer Based Method for Fringe Pattern Analysis," Proc. 1984 SEM Fall Conf. on Exp. Mech., Milwaukee, WI, 61-69 (1984).

10. Plotkowski, P.D., Hung, Y.Y., Hovanesian, J.D. and Gerhart, G., "Improved Fringe Carrier Technique for the Unambiguous Determination of Holographically Recorded Displacements," Opt. Eng., **24**, 754-756 (1985).

11. Beranek, W.J. and Bruinsma, A.J.A., "Geometrical Approach to Holographic Interferometry," EXPERIMENTAL MECHANICS, **20** (9), 289-300 (1980).

12. Kreis, T., "Digital Holographic Interference-Phase Measurement Using the Fourier-transform Method," J. Opt. Soc. Amer., **A3** (9), 847-855 (1986).

13. Kreis, T. and Jüptner, W., "Digital Processing of Holographic Interference Patterns Using Fourier Transform Methods," Measurements, J. Int. Meas. Conf., IMEKO Symp. on Laser Applications in Precision Measurements, Budapest (1986).

14. Savitzky, A. and Golay, J.E., "Smoothing and Differentiation of Data by Simplified Least Squares Procedures," Anal. Chem., **36**, 1627-1639 (1964).

15. Akima, H., "New Method of Interpolation and Smooth Curve Fitting Based on Local Procedures," J. ACM, **17** (4), 589-602 (1970).